Crack formation in tensile InGaAs/InP layers

M. Natali,[a] D. De Salvador,[b] M. Berti, and A. V. Drigo
INFM at the Physics Department, University of Padova, via Marzolo 8, 35131-I Padova, Italy

L. Lazzarini and G. Salviati
CNR-MASPEC Institute, Parco Area delle Scienze 37/A, I-43100 Fontanini-Parma, Italy

G. Rossetto and G. Torzo
CNR-ICTIMA Institute, Corso Stati Uniti 4, I-35127 Padova, Italy

(Received 25 May 2000; accepted 31 July 2000)

A systematic investigation of crack formation has been performed in tensile $In_xGa_{1-x}As$/InP layers with indium composition ranging from $x=0.2$ up to $x=0.35$ and thicknesses ranging from 8 nm to 2 μm. It has been found that cracks form after growth and on a characteristic timescale of several days. The formation of cracks has been found to occur in a well defined thickness interval correlated to the residual strain during growth. Crack formation is favored along the [110] in-plane direction in samples with low indium composition. The results can be rationalized within a model which explicitly takes into account the fact that cracks form after growth. © *2000 American Vacuum Society*. [S0734-211X(00)04705-3]

I. INTRODUCTION

It is now well established that when III–V semiconductor epitaxial layers under low compressive strain exceed a critical thickness an array of misfit dislocations (MDs) are formed at the epilayer–substrate interface. For layers under tensile strain, it has been recently suggested that, the strain relaxation mechanism might be different.[1] In addition to MDs, cracks may form in tensily strained layers and cracks were indeed found to be responsible for strain relaxation in tensile InAlSb/InSb layers by Maigné *et al.*[2] For tensile InGaAs/InP layers in addition to cracks MDs, stacking faults (SF), and twins (TW) have been observed.[3–5] For this system, it is presenly unclear which kind of defects are mainly responsible for strain relaxation.

Concerning the onset of crack formation, a theoretical critical thickness expression has been compared to experimental data on crack formation in tensile strained InGaAlAs/InP and InGaAs/InP layers by Murray *et al.*[6] A good agreement was found by assuming that the samples had relaxed a negligible amount of strain before cracks start to form. However, to our knowledge, no simultaneous investigation of crack formation and strain relaxation has been performed in the literature so far. Moreover, in opposition to the results of Murray *et al.*,[6] in an earlier study Nagai and Noguchi[7] found that cracks form within a misfit interval in liquid phase epitaxy grown tensile InGaAs/InP layers.

An intriguing question relating to crack formation in tensile III–V layers grown on (001) substrates concerns an often encountered preferential formation of cracks along a given ⟨110⟩ in-plane direction. Indeed, since cracks are observed to form on vertical (110) planes they are not affected by the lack of inversion symmetry of the zinc-blende lattice of III–V compounds. Moreover, in Refs. 4 and 5, cracks in tensile InGaAs/InP were observed mainly parallel to [110], while for the same system Franzosi *et al.*[8] reported preferential crack formation along $[1\bar{1}0]$. Similarly Olsen *et al.*[9] observed cracks only parallel to $[1\bar{1}0]$ in tensile InGaP/GaAs layers.

In order to clarify the apparently contradictory behavior of crack formation and to correlate crack formation with strain relaxation we have performed a systematic investigation of cracks as well as of strain relaxation in metalorganic vapor phase epitaxy (MOVPE) grown tensile InGaAs/InP layers.

In a previous work[10] we concentrated on the strain relaxation mechanism. The present work is more oriented to the understanding of crack formation.

II. EXPERIMENT

The samples were grown on (001) semi-insulating InP substrates with an Aixtron AIX200 low pressure reactor. All samples were grown at 650 °C, with a total pressure of 20 mbar and with a V/III ratio of 180. Prior to the InGaAs growth a 500 nm thick InP buffer layer was deposited. The samples were grown in four series of nominally constant indium composition; respectively $x=0.20$, $x=0.25$, $x=0.30$, and $x=0.35$. The measurement of the sample composition (see below) gave the following values: $(20.7\pm0.6)\%$, $(25.5\pm0.4)\%$, $(30.4\pm0.4)\%$, and $(36.1\pm0.9)\%$ where the values represent the average composition and standard deviation of each series. The layer thickness ranged from a few nanometers up to about 2 μm for each series.

The residual strain in the layers was determined by performing high resolution x-ray diffraction (HRXRD) measurements with a Philips MRD diffractometer using Cu $K\alpha$ radiation monochromatized by a Bartels Ge(220) monochromator. Rocking curves were measured of the (004) and (444) Bragg reflections along the four different directions, parallel

[a]Present address: 196 Avenue Henri Ravera, 92225 Bagneux Cedex, France.
[b]Electronic mail: desalvador@padova.infm.it

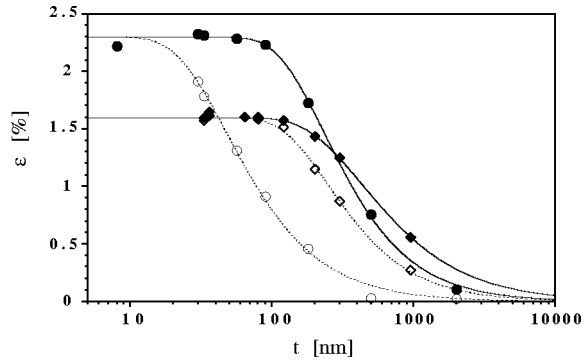

FIG. 1. Residual parallel strain measured along the [110] (open symbols) and $[1\bar{1}0]$ (closed symbols) directions is reported for samples with $x=0.20$ (circles) and $x=0.30$ (diamonds) as a function of the layer thickness t.

to the ⟨110⟩ in-plane axes. The (444) reflection were recorded with grazing incidence angle in order to increase the surface sensivity.

Rutherford backscattering measurements were performed to determine the layer thicknesses as well as the indium composition. Random spectra were recorded with 2 MeV $^4He^+$ beams delivered by the AN-2000 Van de Graaff accelerator at Laboratori Nazionali di Legnaro. During the measurement the sample is tilted 5° from the axial direction and azymuthally rotated around it in order to average channeling effects. The spectra where simulated by an in-house developed computer code which properly takes into account the measurement geometry and the stopping power functions. Trial concentration profiles are tested until a good agreement with the experimental spectrum is achieved.

Cracks were imaged by scanning force microscopy (SFM) with a Park CP model operating in contact mode, using ultralever tips with nominally 10 nm tip radius and nominal aspect ratio 4×1. In contact-mode operation the tip apex wears out quite fast: typical values of effective tip radius of ''used tip'' are in the range of 30–50 nm. In some cases a large number of images of an $80\,\mu m\times80\,\mu m$ size were recorded at different positions on the sample surface to determine the average density of cracks with sufficiently high statistics.

Transmission electron microscopy (TEM) bright field and dark field ⟨110⟩ cross sections (XTEM) were recorded on some selected samples with a JEOL 2000 FX microscope operating at 200 kV on mechanochemically thinned samples finished by room temperature argon ion milling.

III. RESULTS

The results regarding strain relaxation are reported in Ref. 10. Here we recall only the main features of the strain relaxation process: (i) strain relaxation occurs at an epilayer thickness higher than in the compressive case, (ii) strain relaxation is highly asymmetric, the first relaxation direction being the [110], and (iii) the strain relaxation asymmetry increases with increasing misfit, i.e., with decreasing In concentration. As an example Fig. 1 shows the residual strain (ϵ) in the [110] and $[1\bar{1}0]$ in-plane directions for two series of samples grown at $x=20$ and 30 at.%. The asymmetric strain relaxation is shown by the different thickness at which strain starts to relax in the [110] and $[1\bar{1}0]$ directions. In the case of 20 at.% In composition the critical thicknesses relative to the two directions differs by nearly one order of magnitude. This difference is strongly reduced for the series of samples at 30 at.% In composition and nearly vanishes for the 35 at.% In series (not shown).

Typical SFM surface morphology features are shown in Figs. 2(a) and 2(b) for two samples at $x=20$ and 35 at.%,

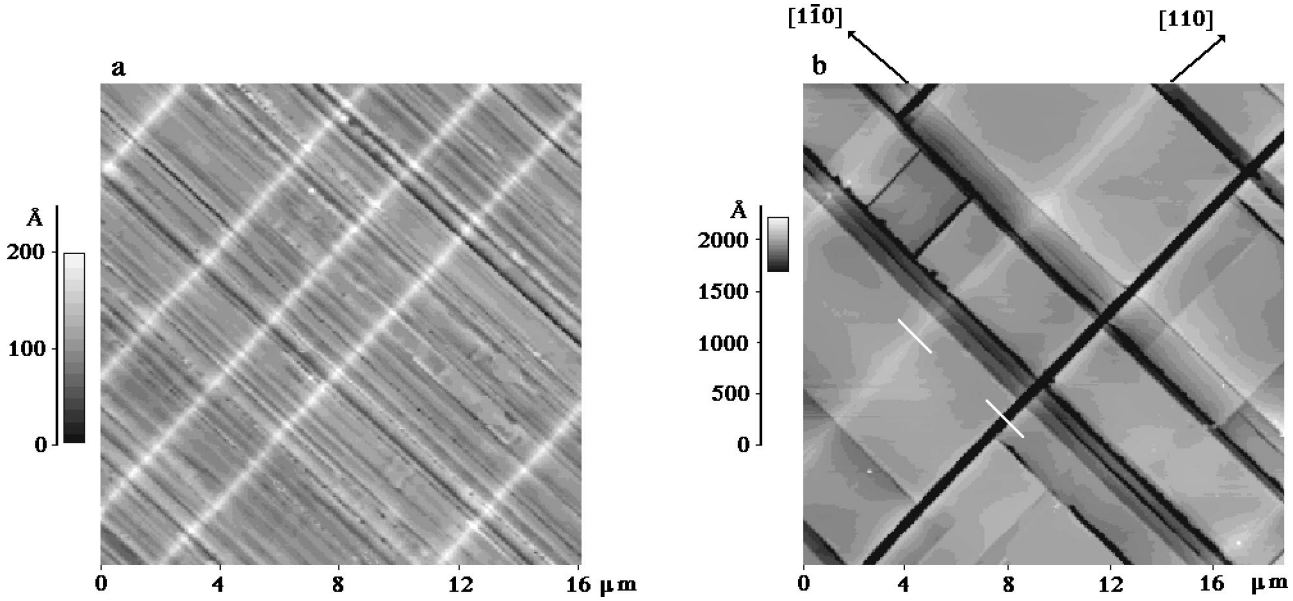

FIG. 2. SFM images are shown for (a) a sample with $x=0.20$ $t=90$ nm and (b) a sample with $x=0.35$ and $t=450$ nm. White lines are crests and were identified as cracks, while dark lines correspond to grooves. The white segments in (b) correspond to the line scans reported in Fig. 3. Note the different gray scale values in (a) and (b).

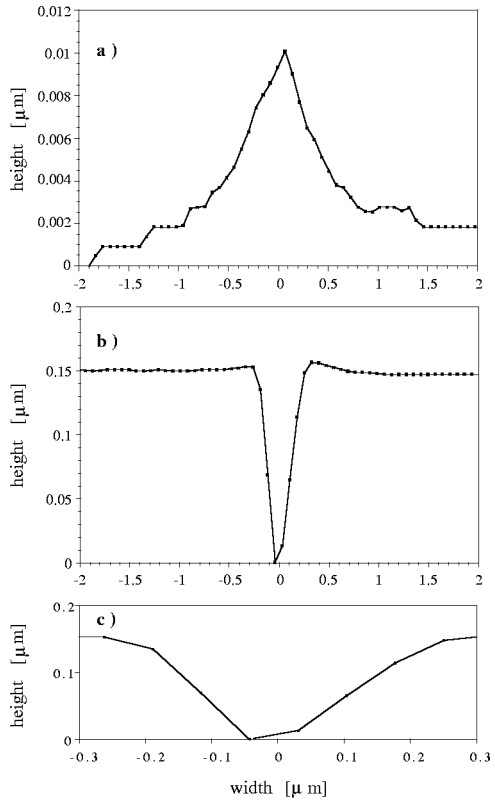

FIG. 3. Line scans of the typical surface features of Fig. 2(b). The line scans of the white and dark features are reported in (a) and (b), respectively. In (c) the line scan in (b) is redrawn with the same scale in the vertical and horizontal axes.

respectively. In Fig. 2(a) straight black features (depressions) are aligned along $[1\bar{1}0]$ while white features (height enhancement) are aligned in the orthogonal [110] direction. At the contrary in Fig. 2(b), relative to a 35% In sample, it is shown that both features (dark and white) occur in both $[1\bar{1}0]$ and [110] directions.

Typical line scans of these two kind of features are reported in Figs. 3(a) and 3(b). They are related to Fig. 2(b) where the line scan intervals are marked by white lines. Figure 3(a) represents the line scan of the white feature which appears to be a height enhancement of about 10 nm, i.e., about 2% of the layer thickness. On the other hand the dark features [Fig. 3(b)] is a groove whose depth is 150 nm, i.e., about one third of the layer thickness.

A central depression on the white features is always detected if a sufficient lateral resolution is adopted in the scan. A high resolution SFM image of the white features is shown in Fig. 4 and suggests the identification of these features as microcracks as shown by the line scan reported in Fig. 5(a). The slope of the depression is mainly determined by the tip aspect ratio. Further confirmation of this fact is given by (110) TEM cross-section images like those reported in Figs. 6(a) and 6(b): the crack is so narrow that it cannot be fully penetrated by the SFM tip. The TEM images show that cracks have {110} side walls and that they penetrate not only the whole epilayer but also the substrate to depths on the order of the epilayer thickness. In most cases it is observed

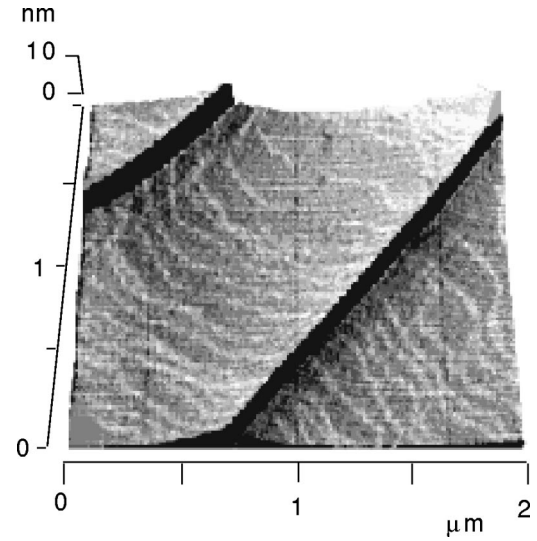

FIG. 4. High resolution SFM image showing two cracks which cut atomic steps on a sample with $x=0.30$ and $t=120$ nm.

that the final part of the crack in the substrate bends to {111} planes as clearly shown in Fig. 6(b). In Fig. 6(c) a *V* groove is also visible. Its dimension and sidewall angles are on the order of those determined by SFM as shown in Fig. 3(c) where the line scan of 3(b) is plotted with the same scale in both *x* and *y* axes. As can be seen, the angle of the side walls is roughly $50°-60°$.

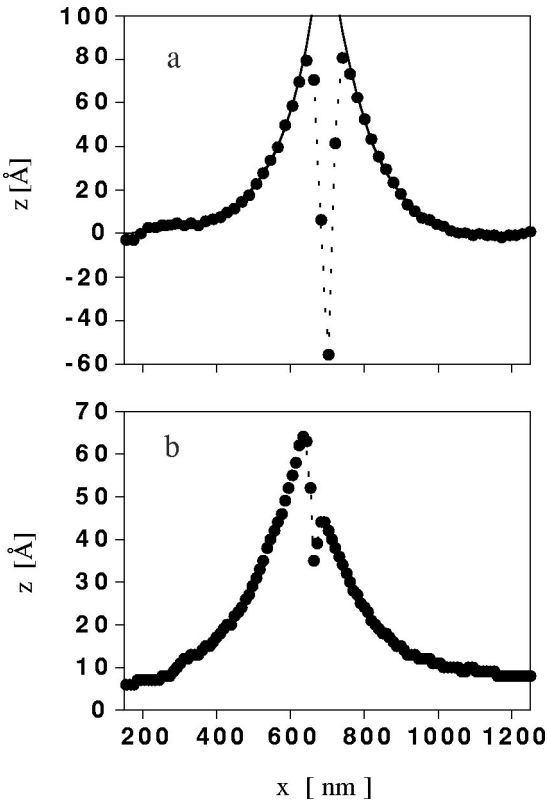

FIG. 5. Typical high resolution SFM line scans of microcracks: (a) symmetric and (b) asymmetric shape of a $x=0.20$ and $t=90$ nm sample. The continuous line in (a) is an exponential fit to the data. The fit decay length is about 110 nm. Dashed lines join the data points.

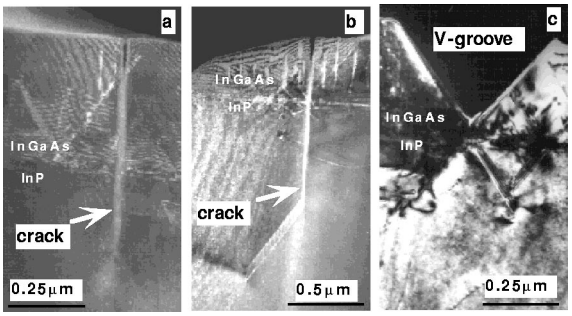

FIG. 6. {110} TEM cross-section images of typical defects for a tensile InGaAs sample with $x=20$ at. % and $t=500$ nm: (a) a crack crosses an extended defect; (b) a crack penetrates the substrate and bends to a (111) plane; (c) *V* groove.

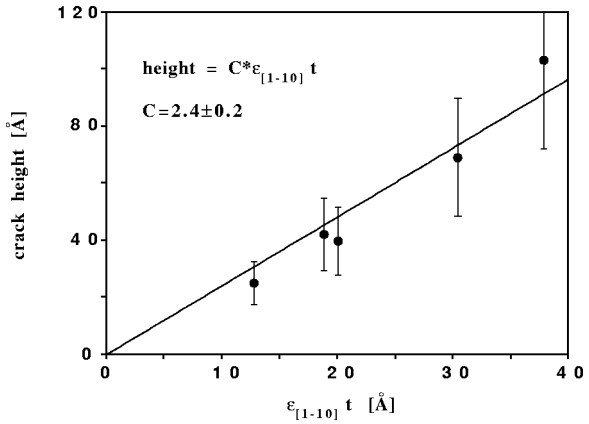

FIG. 7. Average height enhancement at the crack borders in samples of the $x=0.20$ series as a function of the thickness multiplied by the residual strain in the orthogonal direction. The error bars are the standard deviations in the measured crack population.

We summarize here the evolution of the sample morphology as a function of the epilayer thickness. Independently of the In composition, grooves appear first in the $[1\bar{1}0]$ direction at a thickness where strain relaxation in the orthogonal [110] direction is observed by HRXRD. By increasing the layer thickness grooves also appear along the [110] direction again in correlation with significant strain relaxation in the orthogonal direction. The length of the [110] grooves is generally shorter than that in the $[1\bar{1}0]$ direction, as shown in the upper left corner of Fig. 2(b).

In the 20% In composition series microcracks are observed only in the [110] direction. However, for the other composition series cracks are observed in both directions even though the density of the [110] oriented cracks is always higher than the $[1\bar{1}0]$ density. Contrary to the groove behavior, cracks are observed in a limited range of the epilayer thickness, independently of the indium composition.

Having identified the white features of Fig. 2 as microcracks, we address the question of why cracks are associated to a height enhancement. It could be due either to elastic strain relaxation or to enhanced overgrowth in the strain relaxed regions around the crack. Thus, we investigated in detail the height enhancement features. First of all we note that the height enhancements shown in Fig. 5 are on the order of several nanometers, i.e., nearly 2 orders of magnitude smaller than the epilayer thickness. Then we observe that sometimes the height enhancement on the two sides of the crack is asymmetric [Fig. 5(b)] and in other cases it is symmetric [Fig. 5(a)]. Even though it is not possible to directly correlate SFM topographs to XTEM micrographs, we attribute this different behavior to cracks penetrating the substrate with and without bending, respectively. In both cases the height enhancement decays exponentially with increasing distances from the crack with a characteristic length on the order of the epilayer thickness. This fact is in favor of elastic strain relaxation. From a rough strain relaxation model, where the crack penetrates only the layer thickness and causes uniaxial and total strain relaxation near the walls of the crack, it is expected that the height enhancement is proportional to the strain in the direction perpendicular to the crack multiplied by the layer thickness. In Fig. 7 we report the average height enhancement of the cracks measured on different samples of the 20 at. % In series as a function of the strain-thickness product. The data points show a very nice linear correlation as expected. However, the slope shown in Fig. 7 is about four times larger than that expected from this simple strain relaxation model. This discrepancy could be reduced by nearly a factor of 2 by considering that the crack penetrates the substrate inducing compressive strain in the substrate and thus contributing to the height enhancement.

Even though inconclusive, the above reported observations are in favor of elastic strain relaxation around the crack. This fact raises the question whether the cracks form during (as soon as a critical thickness is reached) or after growth. In the high resolution SFM images of Fig. 4 it can be observed that atomic steps on both sides of the crack are correlated, strongly suggesting that cracks form at the end of or after growth. A further confirmation of this hypothesis comes from the XTEM micrograph in Fig. 6(a) where the crack is shown to cut an extended defect (stacking fault) that could not propagate across an existing crack.

In order to have direct evidence of the time evolution of crack formation, on one 20% In sample we measured the crack density in SFM topographs immediately after growth and at successive different times after growth. The results are shown in Fig. 8. The data points show a significant increase of the crack density with time after growth, and this directly confirms that cracks form after growth.

The data points may be fitted by the expression

$$\rho=\rho_{\infty}(1-e^{t/\tau}), \tag{1}$$

where ρ is the crack density, t is the time elapsed after growth, τ is the characteristic time scale of the formation process, and ρ_{∞} is the saturation density. From the data in Fig. 8 we find a characteristic timescale of about ten days.

A statistical analysis of the spatial frequency of the microcracks (white features in SFM pictures) has been performed by means of homemade macrocode[11] written for SMX, a public domain image analysis software,[12] that detects spikes in line scans taken at different points on the samples and that calculates their average density and height.

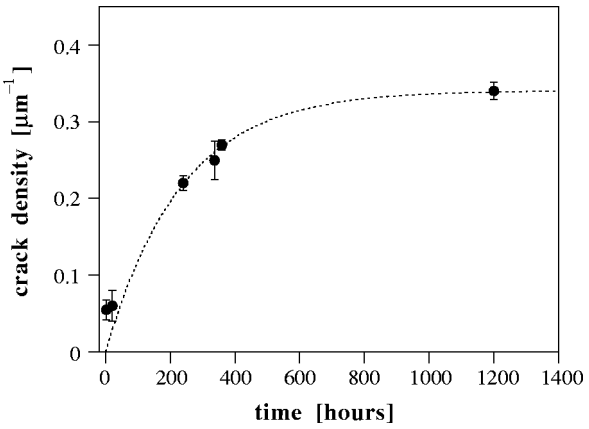

FIG. 8. Crack density as a function of time elapsed after the growth for a sample with $x=0.20$ and $t=73$ nm.

The densities of the [110] oriented microcracks for samples of the 20 and 30 at. % In composition series are shown in Figs. 9(a) and 9(b), respectively. These analyses where performed several months after growth, so that, on the basis of the time evolution shown in Fig. 8, the measured densities are representative of the saturation densities.

From Fig. 9 it appears that the crack density rapidly increases above a given layer thickness, it reaches a maximum and then, by increasing the layer thickness, it decreases until it vanishes. As it is difficult to imagine a filling mechanism leading to the crack disappearance, this behavior is further confirmation of crack generation after growth. Moreover, it suggests that their nucleation is related to the residual strain after growth.

Another important point is whether or not the cracks induce strain relaxation. In order to investigate this point, strain measurements were performed just after growth and repeated several months later on the 20 at. % In 90 nm

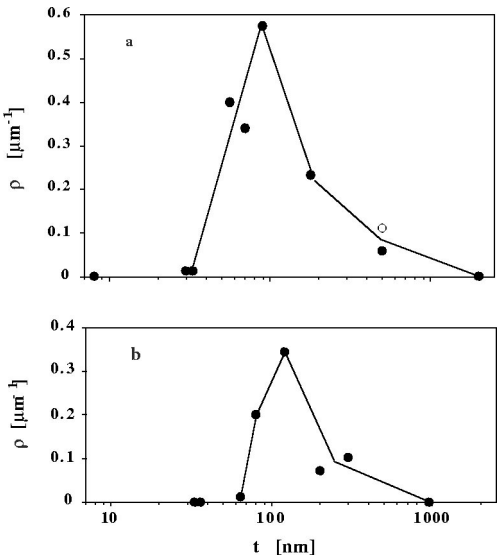

FIG. 9. Linear density of cracks parallel to [110] as a function of the layer thickness for (a) $x=0.20$ and (b) $x=0.30$. Closed circles refer to SFM analyses. The open circle in (a) corresponds to XTEM analysis.

sample with the highest revealed crack density along the [110] direction (see Fig. 9). The [110] strain keeps the constant value of about 0.9% as expected from the fact that no crack forms along the $[1\bar{1}0]$ direction. On the contrary the $[1\bar{1}0]$ strain drops from 2.21% to 1.78% during the process. This means that, even in the case of the highest crack density, only a small fraction (about 20%) of the strain is relaxed by cracks. It is worth noting that all the other HRXRD measurements in this work were made within two days of sample growth and therefore the strain behavior reported in Fig. 1 does not account for relaxation due to crack formation.

The above reported results can be summarized as follows: (i) strain relaxation is increasingly asymmetric with increasing misfit, (ii) cracks are formed *after* growth, (iii) the crack density increases with time after growth and saturates with a timescale on the order of ten days, and (iv) cracks do not lead to a complete strain relaxation.

IV. DISCUSSION

One of the most important question to address is the existence and the functional dependence of a critical thickness for crack formations. The only model present in the literature to describe crack formation onset is due to Murray *et al.*[6] who proposed an energy balance between the increase of surface energy due to the crack walls and the elastic energy relaxed in the epilayer around the crack. The final form of their model is $f^2t=C$, where f is the misfit of the layer and C is a constant which depends on the surface energy and on the elastic constants. In order to calculate the C constant the cracks are assumed to penetrate only the layer and not the substrate. Moreover, full strain relaxation is assumed to occur uniformely in two areas of height t and width t on both sides of the crack.

Taking into account that cracks form after growth, the misfit must be substituted by residual strain. Since we have shown that strain relaxation is strongly asymmetric, one can expect asymmetric crack distributions, as indeed was observed. The whole phenomenology described in this article enormously complicates a quantitative description. First of all, the strain is no more biaxial and the appropriate expression for the energy density should be used. Second, the crack penetrates the substrate (sometimes bending) and the strain and energy modifications induced by its nucleation must include the appropriate portion of the substrate. Finally, our results in Fig. 5 indicate that the dependence of the strain relaxation as a function of the distance from the crack is much more complicated than that assumed in Ref. 6.

These difficulties could be overcome only by a finite element method (FEM) calculation. As a matter of fact, for the more simple problem of the elastic energy released near the free border of an epitaxial layer, Jain *et al.*[13] have shown that this calculation can be performed to a reasonable accuracy only with FEM.

In view of these difficulties we try to experimentally derive an expression for the critical thickness of crack formation. We assume that the driving force is related to the strain energy. As a crack in the direction $[1,\pm1,0]$ relaxes strain

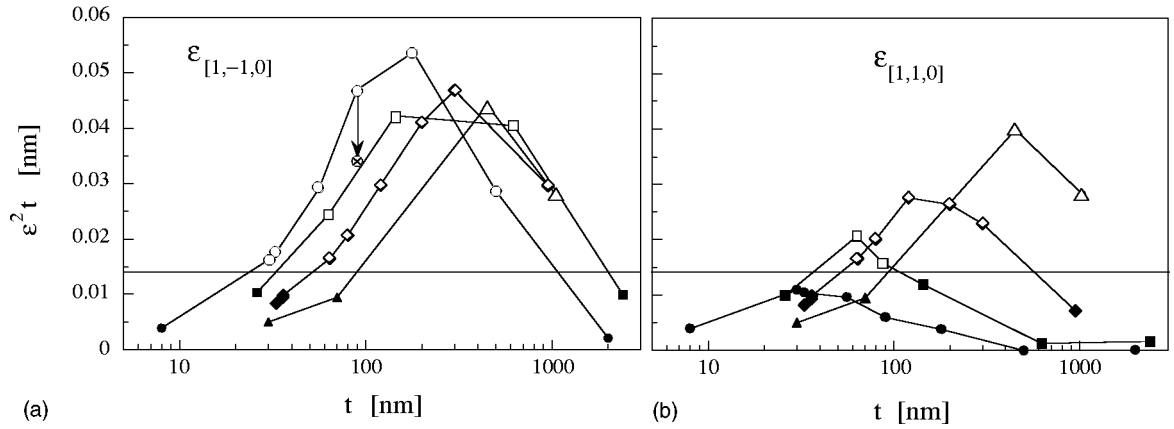

FIG. 10. Squared residual strain along (a) $[1\bar{1}0]$ and (b) [110] multiplied by the layer thickness as a function of the thickness for the samples of the four composition series: circles, $x=0.20$; squares, $x=0.25$; diamonds, $x=0.30$; triangles, $x=0.35$. Open and closed symbols refer to samples where cracks were and were not observed, respectively. The horizontal line represents the onset value for crack formation: (0.014 ± 0.002) nm. The arrow indicates the decrease of $\epsilon^2 t$ from the value just after the growth (open circle) to the value measured after crack saturation (crossed circle) for the sample with the highest crack density.

mainly in the orthogonal $[1,\mp1,0]$ direction, we assume that the relevant energy term is proportional to $\epsilon^2_{[1,\mp1,0]}t$ where the strain $\epsilon_{[1,\mp1,0]}$ is that determined just after the growth.

In Fig. 10(a) we plot $\epsilon^2_{[1\bar{1}0]}t$ as a function of the thickness for all samples. Open symbols indicate the presence of cracks in the [110] direction, full symbols indicate that no cracks are observed in the same direction. In Fig. 10(b) the same plot is made using the strain $\epsilon_{[110]}$ and considering the crack formation along the $[1\bar{1}0]$ direction. As can be seen in both plots, the samples with cracks can be well separated by the samples with no cracks by a line drawn at about $\epsilon^2 t$ equal to 0.014 nm. In other words all our results are explained by the fact that cracks form after growth and they are well described by the following empirical equation for crack formation:

$$\epsilon^2 t > (0.014\pm0.002)\,\text{nm}, \tag{2}$$

where ϵ is the residual strain in the direction perpendicular to the cracks formation.

In fact there are no cracks in the $[1\bar{1}0]$ direction for the 20 at.% series because the strain relaxation in the perpendicular direction occurs by means of other defects at small values of the thickness so that $\epsilon^2_{[110]}t$ never reaches the critical value. Furthermore, the existence of a thickness interval for crack formation, well illustrated by Fig. 9, is explained by the strain relaxation during growth for large layer thicknesses where the residual strain decreases rapidly and the strain energy falls below the critical value. We stress here that knowledge of the residual strain is of fundamental importance to predict the formation of cracks. Therefore, some of the contradictory results reported in the literature could be explained by particular features of the strain relaxation process in those experiments.

The critical thickness defined by Eq. (2) could be read as an equilibrium formula for crack formation. Above the critical value there is a sufficient amount of free energy in order to *propagate* new cracks relaxing strain until $\epsilon^2 t$ falls below the critical value. However, the results in Fig. 10(a) clearly show that this does not happen for the sample with the highest crack density (20 at.% In, 90 nm). For this sample $\epsilon^2 t$ is well above the critical value even after crack saturation: the arrow indicates the decrease from the value just after the growth (open circle) to the value measured at crack saturation (crossed circle).

Two are the possible explanations of this problem: (i) cracks interact in some way which prevents further crack formation and (ii) cracks have a high nucleation energy barrier which can be exceeded only in a finite number of sites, i.e., crack formation is an heterogeneous nucleation process. The first interpretation seems to be quite improbable because the minimum crack distance is at least one order of magnitude greater than the height decay length that can be used as a typical interaction length. According to the second interpretation crack formation is kinetically limited and the generation rate cannot be accounted for by referring only to the average elastic strain energy density in the layer: there must exist a number of local stress concentrators which provide sufficient energy to overcome the high nucleation barrier. This point of view allows us to understand the time evolution of the crack density. Equation (1) can be interpreted by assuming that cracks develop from a fixed number of sites with a probability per unit time $1/\tau$. Once all crack sources are exhausted the crack density saturates, notwithstanding the fact that the residual strain in the layer is still high enough to allow propagation of more cracks.

An other important question is: why do cracks not form during growth? The answer probably lies in the much longer timescale for crack formation compared to that for generation of misfit dislocations, stacking faults, or twins. This is reasonable since crack formation involves the breaking of atomic bonds distributed on a surface while MDs and SFs observed in InGaAs/InP involve broken bonds only along the lines corresponding to the core of dislocations. Moreover, while the mobility of MDs decreases drastically as the tem-

perature is lowered from growth temperature to room temperature, this does not occur for cracks which do not require thermal activation for their propagation. In other words it appears that tensily strained InGaAs layers have a transition from plastic to fragile behavior when the temperature is decreased. At room temperature strain energy is necessary to propagate the cracks (as described by our model); however, the high nucleation energy barrier can be exeeded only by local perturbations.

V. CONCLUSION

Crack formation has been systematically investigated in tensile InGaAs/InP(001) layers grown by metalorganic chemical vapor deposition. We found that cracks form after growth with a characteristic timescale of several days and within a thickness interval. An empirical formula for the crack critical thickness is proposed. This formula relates the crack formation to the residual strain after growth. By explicitly considering the fact that cracks form after growth and by using the measured residual strain values we were able to rationalize the formation of cracks within a thickness interval as well as the crack formation only along [110] for 20 at. % samples.

Crack formation was found not to be an equilibrium process but to be determined by the availability of local stress concentrators which act as crack sources. In fact, the strain relaxation due to cracks is low and it does not lead the strain energy below the critical value for crack formation.

ACKNOWLEDGMENTS

The authors wish to thank A. Camporese for technical support during the MOVPE growth and G. Carta and A. Coati for some of the XRD measurements.

[1]P. Maigné, M. Gendry, T. Venet, Y. Tahri, and G. Hollinger, Appl. Phys. Lett. **69**, 682 (1996).
[2]P. Maigné, M. W. C. Dharma-Wardana, D. J. Lockwood, and J. B. Webb, J. Appl. Phys. **77**, 1466 (1995).
[3]R. Hull, R. A. Logan, B. E. Weir, and J. M. Vandenberg, Appl. Phys. Lett. **63**, 1504 (1993).
[4]G. Wagner, V. Gottschalch, R. Franzheld, S. Kriegel, and P. Paufler, Phys. Status Solidi A **146**, 371 (1994).
[5]A. Dieguez, A. Villa, A. Cornet, S. A. Clark, D. I. Westwood, and J. R. Morante, J. Vac. Sci. Technol. B **15**, 687 (1997).
[6]R. T. Murray, C. J. Kiely, and M. Hopkinson, Philos. Mag. A **74**, 383 (1996).
[7]H. Nagai and Y. Noguchi, Appl. Phys. Lett. **29**, 740 (1976).
[8]P. Franzosi, G. Salviati, M. Scaffardi, F. Genova, S. Pellegrino, and A. Stano, J. Cryst. Growth **88**, 135 (1988).
[9]G. H. Olsen, M. S. Abrahams, and T. J. Zamerowsky, J. Electrochem. Soc. **121**, 1650 (1974).
[10]A. V. Drigo, M. Natali, M. Berti, D. De Salvador, G. Rossetto, G. Torzo, G. Carta, L. Lazzarini, and G. C. Salviati, in *Lattice Mismatched Thin Films* edited by E. A. Fitzgerald (TMS, Cambridge, MA, 1999), pp. 153, 162.
[11]D. Cerolini, Degree thesis, 1998, Padova University, unpublished.
[12]http://reg.ssci.liv.ac.uk/
[13]S. C. Jain, A. H. Harker, A. Atkinson, and K. Pinardi, J. Appl. Phys. **78**, 1630 (1995).